LDPC CODED VISIBLE LIGHT COMMUNICATION

by

Merve Apalak

APPROVED BY SUPERVISORY COMMITTEE:

Dr. Kamran Kiasaleh, Chair

Dr. John P. Fonseka

Dr. Issa M.S. Panahi

Dr. Lakshman Tamil

To my mother.

LDPC CODED VISIBLE LIGHT COMMUNICATION

by

MERVE APALAK, BE

THESIS

Presented to the Faculty of

The University of Texas at Dallas

in Partial Fulfillment

of the Requirements

for the Degree of

MASTER OF SCIENCE IN

ELECTRICAL ENGINEERING

THE UNIVERSITY OF TEXAS AT DALLAS

August 2018

ACKNOWLEDGMENTS

It has been a pleasure and a rewarding learning experience to complete my master's degree under the supervision of Dr. Kamran Kiasaleh. I appreciate Dr. Kamran Kiasaleh for leading me to novel research problems. In so many ways he has helped me to build my research skills and put my research in a broad scope by indicating critical parts, emphasizing similarities and contradictions to other works. I want to express my gratitude to Dr. John Fonseka. His support, kindness, endless enthusiasm, and generosity of heart motivated me during the first part of my research. I thank the members of my supervisory committee, Dr. Issa Panahi and Dr. Lakshman Tamil for their valuable insights and recommendations on my research.

I would like to thank Mr. Serkan Tokgoz. I am deeply indebted to him. He has stood by me during this difficult journey and helped me more than anyone. Our talks and brain storming have sparked a new dimension that completely changed my attitude about being an engineer and doing research.

I am very thankful to my former and current coworkers Mrs. Elahe Rezaei and Mr. Nima Taherkhani. When I was faced with difficulties in my research, they appeared with their patience and kind support. It has been an amazing experience to work with dedicated and ingenious people around me.

Needless to say, I am forever indebted to my parents. I am very fortunate to have them. I have aimed to please them with my success from the day I decided my future goals. Their endless love, support, trust and encouragement has brought me to today. Finally, I want to thank the Turkish Ministry of National Education for providing me financial support during my master.

July 2018

LDPC CODED VISIBLE LIGHT COMMUNICATION

Merve Apalak, MSEE
The University of Texas at Dallas, 2018

Supervising Professor: Dr. Kamran Kiasaleh

Visible light communication (VLC) using the visible light band in the electromagnetic spectrum (EM) promises an opportunity to reach a significantly large and unregulated part of the EM spectrum. Therefore, this modality of communication has become a promising alternative to radio frequency (RF) communication, which is falling short in responding to the future demands for spectrum. Recent studies have shown that the direct detection optical orthogonal frequency-division multiplexing (DDO-OFDM) can increase throughput of VLC system with proper double-sided clipping. Low density parity check codes (LDPC) are shown to be capacity achieving error correcting codes. In this thesis, LDPC codes are implemented to mitigate the clipping noise in VLC systems in order to promote spectrum efficiency. The impact of clipping range is studied, and optimum range is suggested. In addition, puncturing is applied for different coding rates to maximize the capacity of the channel by reducing the effect of clipping. Finally, the performance enhancement of the LDPC coded visible light scheme is compared with that of the Reed Solomon coded VLC systems.

TABLE OF CONTENTS

ACKNOWLEDGMENTS v

ABSTRACT vi

LIST OF FIGURES viii

CHAPTER 1 INTRODUCTION 1

1.1 Motivation 1

1.2 Contribution 4

1.3 Outline of Thesis 5

CHAPTER 2 VISIBLE LIGHT COMMUNICATION 7

2.1 Introduction 7

2.2 Advantages of Visible Light Communication 7

2.3 Principles of Optical Communication 9

2.4 Modulation Techniques 11

2.5 Summary 15

CHAPTER 3 LOW DENSITY PARITY CHECK CODE 16

3.1 Linear Block Codes 16

3.2 Matrix and Graphical Representation of LDPC Code 18

3.3 Encoding 21

3.4 Iterative Decoding of LDPC Codes 24

3.5 LDPC Code Construction 28

3.6 Puncturing of LDPC Codes 30

3.7 Conclusion 31

CHAPTER 4 SYSTEM MODEL AND SIMULATION RESULTS 33

CHAPTER 5 CONCLUSION 40

REFERENCES 42

BIOGRAPHICAL SKETCH 46

CURRICULUM VITAE 47

LIST OF FIGURES

Figure 2.1 Electromagnetic Spectrum.....9

Figure 2.2 OWC transmission link. Transmitter and receiver is shown with basic components in LOS and NLOS scenarios.....10

Figure 2.3 Optical wireless channel model is given.....10

Figure 2.4 Illustration of frequency spectra formats of multi-carrier (on the left) and single carrier (on the right).....12

Figure 2.5 The structure of transmitter and receiver for O-OFDM.....13

Figure 3.1 Systematic format of a codeword.....18

Figure 3.2 Regular (3,6) LDPC code showing Tanner graph and H, parity check matrix.....19

Figure 3.3 Approximate upper triangular form for H.....21

Figure 3.4 Greedy algorithm flow chart.....23

Figure 3.5 First half iteration and second half iteration in Message-Passing Algorithm.....25

Figure 3.6. BER performance of LDPC codes with block length of 1008. Red curve depicts 0.6 rate punctured LDPC code. Blue curve is the original half rate LDPC code.....31

Figure 4.1 16-QAM bit error rate performance of LDPC coded DCO-OFDM vs RS encoded DCO-OFDM in AWGN channel for different clipping ranges.....34

Figure 4.2. 16-QAM Bit error rate performance of LDPC coded DCO-OFDM vs RS encoded DCO-OFDM in AWGN channel with puncturing.....36

Figure 4.3. 64-QAM Bit error rate performance of LDPC coded DCO-OFDM vs RS encoded DCO-OFDM in AWGN channel for different clipping ranges.....37

Figure 4.4. 64-QAM bit error rate performance of LDPC coded DCO-OFDM vs RS encoded DCO-OFDM in AWGN channel with different puncturing rates.....38

CHAPTER 1

INTRODUCTION

1.1 Motivation

Radio Frequency (RF) networks take an important place in our daily lives. According to the mobile data traffic analysis, as demand of data usage increases, the spectrum used by RF communication will become heavily congested. It is important to note that the limitations of the regulated RF spectrum will eventual lead to saturation in the capacity that such networks can offer. Therefore, a complementary technology to RF communication will be required. Visible light communication (VLC) is introduced as a developing technology which has many advantages over RF communication. The first discovery using visible lights traces back to the well-known photophone experiment by Alexander Graham Bell [1]. He modulated the voice signal onto the sunlight and transmitted the signal over 200 meters. Gfeller and G. Bapst's research demonstrated indoor optical wireless communication by diffused infrared radiation [2]. VLC requires high-speed light emitting diode (LED) to be competitive in the wireless domain. For this reason, VLC or infrared communication channels using LEDs were limited to low-speed applications, such as remote controls, etc. The development of high-speed LEDs has allowed the realization of VLC systems that can be competitive to RF wireless in short range communications, such as indoor venues, which are primarily connected via Wi-Fi technology. The first fundamental study of VLC was accomplished by S. Haruyama and M. Nakagawa. They put forward a concurrent illumination and communication system using white LEDs [3]. Later on, variety of novel studies were carried out, such as operating LED traffic lights to transmit traffic information and 2-dimensional image

sensor. Komine *et al.* [4] discussed narrowband OFDM implementation though white LEDs which creates a path for recent VLC research.

In general, VLC systems use LED intensity to carry the data information wirelessly. The intensity of the light remains a positive term. Therein lies the issue with VLC systems as communication signals are expected to take on both positive and negative values. LEDs also are inherently nonlinear. Optically power efficient OFDM signals were designed with a new technique in [5]. Since OFDM signals suffer from large peaks (large peak to average power ratio) it is expected that the transmitting LED will clip the OFDM signal. This fact combined with the fact that the modulating signal that is presented to LED cannot have a negative value result in a double-clipping of the OFDM signal. Clipped OFDM signals show optical power efficiency rather than conventional OFDM signals as the range of the signal is controlled by LED. On the other hand, clipping process distorts the transmitting signal and results in performance degradation. Hence, mitigating the impact of nonlinear distortion has become a focus of researches [6,7,8]. Recently, VLC OFDM employing Reed Solomon (RS) coding is presented to mitigate the impact of clipping noise [9]. In this study, it is shown that decreasing the clipping affect at the transmitter by using puncturing on the OFDM carriers enhances the system bit error rate (BER) performance.

In systems where error control coding is utilized, minimizing the SNR requirement to achieve a specific error rate is the ultimate goal. This approach maximizes the information rate with a bound that that was developed by Shannon [10]. LDPC codes were first proposed by Robert Gallager in 1963 [11]. Unfortunately, due to its decoding complexity, the engineering community did not pay much attention to this seminal work. Later, Tanner [12] in a landmark paper described a graphical model notation for constructing LDPC codes. Recent excitement about LDPC codes was sparked

by Mackay and Neal who demonstrated that LDPC codes with iterative decoding, based on belief propagation also known as sum-product algorithm, have an error performance that leads to an information rate near Shannon limit [13]. Sae-Young Chung *et. al.* suggested that well designed LDPC codes have an outstanding capacity approaching performance within 0.0045dB of Shannon Limit [14]. While parity check matrix of LDPC code is constructed, stopping sets and girths have a crucial impact on the convergence of LDPC codes. In order to reach a large girth in Tanner graph, progressive edge growth construction technique was invented in [15]. PEG construction has a notable outcome on encoding complexity and code performance because it is progressively established in a best-effort sense. In addition to that, it is often desirable in communication systems to have the capability of accommodating various code rates in order to deal with changing channel conditions. This mode can be adapted to the changing conditions of the time varying channels while using the same encoder/decoder pair which is known as a rate compatible code. [16]. Randomly punctured codes are mentioned in [17] which provide the system with high code rate while transmitting fewer code symbols. It was also proved that randomly punctured LDPC codes have asymptotically good performance when minimum distance analysis is conducted. Therefore, when low rate LDPC decoder is used, puncturing LDPC codes is advantageous for longer block length code with large sparse matrices and large minimum distances.

In VLC, optical wireless channel (OWC) is a time-invariant channel (no fading as it is typically for indoor applications). Ambient light in environment and circuit noise in components are the main sources of interference in the optical wireless channels (OWC). Moreover, thermal noise and shot noise are taken in to consideration when noise sources are modeled. These two independent signals can be modeled as additive white Gaussian noise (AWGN). Therefore, the OWC systems

can be studied when forward error correction (FEC) coding is utilized using AWGN analysis. In a nutshell, the high capacity of the VLC channels and the capacity achieving LDPC codes presented in [17] offer us with a new field of study that focuses on the use of LDPC codes in VLC systems to enhance performance in the presence of clipping.

1.2 Contribution

This thesis concentrates on the analysis of LDPC coded VLC systems with and without puncturing when signal clipping is present at the transmitter. The proposed system is compared with RS coded VLC systems in terms of bit error performance.

- First, the well-known OFDM which can achieve high capacity is implemented with LDPC coding.
- Optical OFDM signal which uses Intensity Modulation/Direct Detection (IM/DD) must be non-negative and real. This constraint indicates that bias terms must be added to guarantee a positive signal for intensity modulation. Therefore, DC-biased optical-OFDM (DCO-OFDM) method is implemented. Constraining QAM symbols to have Hermitian symmetry on the active carriers produces a real-valued time domain signal in DCO-OFDM. Later to satisfy the non-negative rule, DC bias is added on bipolar time domain signals. While large signal constellation used, high-valued DC bias is required. However, high Peak to Average Power Ratio (PAPR) is reduced by clipping which occurs at zero for negative parts of the signal. However, the peak values are clipped due to the peak voltage an LED can accept.
- LDPC encoded data vector with DCO-OFDM is proposed for reducing the severe impact of clipping, which can improve the error caused by non-linear distortion of the LED.

- Performance of progressive edge growth is studied. It is shown, via simulation, that PEG code construction with LDPC coded VLC systems outperforms RS coded VLC systems in some scenarios.
- Finally, performance of punctured LDPC coded VLC structure is compared with the performance of punctured Reed Solomon coded VLC with double-sided clipping. Puncturing process turns in to an advantage for the VLC system to control clipping probability.

1.3 Outline of Thesis

The remainder of the thesis is organized as follows.

Chapter 2 outlines a brief overview of the evolution and fundamentals of wireless communication where RF and OWC are discussed.

In Chapter 3, VLC systems are discussed. Advantages of VLC and the constraints due to LED front-end are described in this chapter. Characteristics of LED are discussed in Section 3.1. Mathematical details of the O/E conversion in the multi-carrier modulation schemes, such as M-QAM DCO-OFDM, under illumination requirements are discussed in this chapter.

In Chapter 4, the basic terminologies of LDPC codes are introduced. First, a general introduction to linear block codes is provided. Subsequently, matrix and graphical representation of LDPC codes via regular and irregular matrixes with polynomial distribution are discussed. The Tanner graph is also introduced. Mathematical representation of encoding process and complexity analysis are presented in Sections 4.2 and 4.3. In addition, sum product decoding and construction of PEG

is discussed in this chapter. Finally, performance of punctured LDPC codes is compared with that of the regular LDPC codes.

Chapter 5 presents a summary of Reed Solomon coded VLC systems. We discuss the achievable information rates for LDPC coded DCO-OFDM for AWGN channel under minimum, average and maximum optical power constraints. These results are compared with those of Reed Solomon coded VLC systems.

Chapter 6 concludes the thesis and suggests future works.

CHAPTER 2

VISIBLE LIGHT COMMUNICATION

2.1 Introduction

In recent years, VLC systems using LEDs and photodiodes as transceivers to convey information have been gaining importance due to proliferation of LEDs for interior illumination. Moreover, VLC is envisioned as a complementary or an alternative to RF communication. This chapter discusses VLC and conventional RF communication differences under various conditions. In section 2.2, state of the art VLC systems are described. In section 2.3, optical wireless channel and its constraints are addressed. Finally, in section 2.4, modulation techniques for VLC are introduced, and mathematical models are presented.

2.2 Advantages of Visible Light Communication

In the last few decades, wireless industry has witnessed a remarkable growth in the user demand for capacity. Wireless platforms, such as smart phones, smart watches, laptops, and tablets, have increased demand on connectivity by orders of magnitude. Although allocation of new spectrum can offer a temporary relief, new modalities in communication must be explored to meet the enormous demand for capacity. VLC, which principally is being deployed worldwide for the illumination of infrastructures, offers an avenue to provide wireless connectivity without imposing any additional burden on the congested RF spectrum. VLC, in general, has some advantages over RF communication [18]. These advantages are as follows.

- *Limited RF spectrum versus wide spectrum of visible light*: Visible light spectrum range is between 400THz -800THz and radio frequency range is between 3kHz to 300 GHz. Due to proliferation of wireless devices, a large portion of electro-magnetic RF spectrum of is already occupied. VLC delivers an unlicensed and unused spectrum range which offers a solution for limited spectrum of radio waves. Figure 2.1 shows the electromagnetic spectrum; visible light spectrum is 4 orders of magnitude larger than that of radio waves. Although developments for terahertz frequency range (from 100 GHz to 10 THz), known as millimeter wave (mm-wave) communication, are reported in [19], new infrastructure would be required for this wavelength band. The cost of implementation is also another drawback of mm-wave systems. To the contrary, light emitting diodes are inexpensive and have already been deployed for lighting purposes. It is reported that 10 billion led bulbs can be reused and operated as VLC transmitters.
- *Interference and security*: Since light cannot penetrate through the opaque objects, visible light communication can be provided just for the users in confined areas with enhanced security. Therefore, the signal isolation property prevents an access of unauthorized person in VLC communication areas. Moreover, robustness to electromagnetic interference is a powerful feature of VLC. Furthermore, VLC can be deployed in environments where RF signals can interfere with the functions of sensitive equipment. For that reason, VLC becomes a perfectly suitable alternative to RF systems in hospitals, airplanes and aerospace applications [20].
- *Energy efficiency, safety and low-cost LEDs:* LEDs are widely deployed since they are fast, energy efficient and eco-friendly compared with the conventional lightening. It is possible

that VLC components can be made small and compact. Hence, LEDs can be efficiently employed into the current infrastructure. Furthermore, there are no health hazards to human body caused by visible light radiation at low power levels. On the other hand, RF electromagnetic waves are considered as a possible reason for cancer [21].

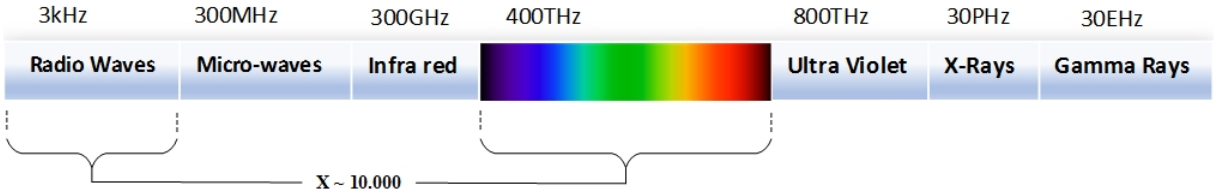

Figure 2.1. Electromagnetic Spectrum

2.3 Principles of Optical Communication

2.3.1 Optical Channel and Front-ends

As opposed to conventional communication channel, optical wireless channel (OWC) enjoys several different features. OWC is proposed as a linear, time-invariant and memoryless system. Figure 2.2 depicts an OWC link. Transmission happens as follow: transmitter → optical wireless channel → receiver which is similar to RF transmission. In Figure 2.2, transmitter block is responsible for processing the digital signal and converts to an analog current signal using a digital signal processor (DSP). Analog current signal drives the LED. Information carrying current signal is transformed into optical intensity in the transmitter. Later, the optical signal is passed though the OWC. The objects in the environment absorb a portion of the power of optical energy, and the rest is reflected. Here, between the transmitter and the receiver the transmission link can be classified into two categories, which are line-of-sight (LOS) link and non-line-of-sight (NLOS) link. LOS and NLOS links signal components are both captured by the receiver. Electrical current,

$y(t)$, is extracted from optical signal in the photodiode (PD). The detected signal is amplified and the demodulator converts the received signal into binary date [22]. In a nutshell, electrical to optical (E/O) and optical to electrical (O/E) transformation allows for the use of LEDs to exchange information.

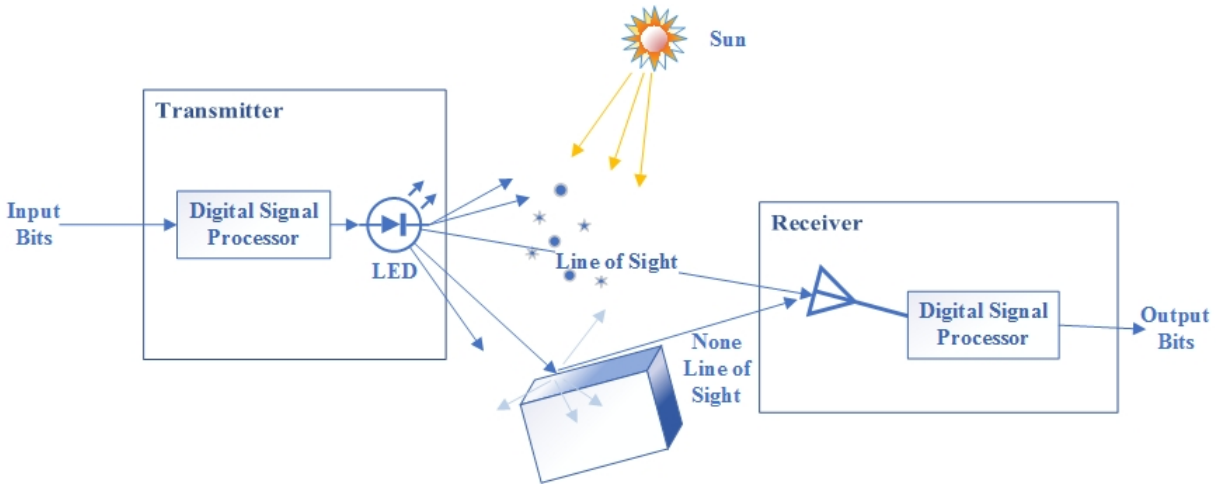

Figure 2.2. OWC transmission link. Transmitter and receiver is shown with basic components in LOS and NLOS scenarios.

The system model of OWC is illustrated in Figure 2.3 and proposed by Kahn in [23]

$$y(t) = h(t) * I(t) + w(t) \tag{2.1}$$

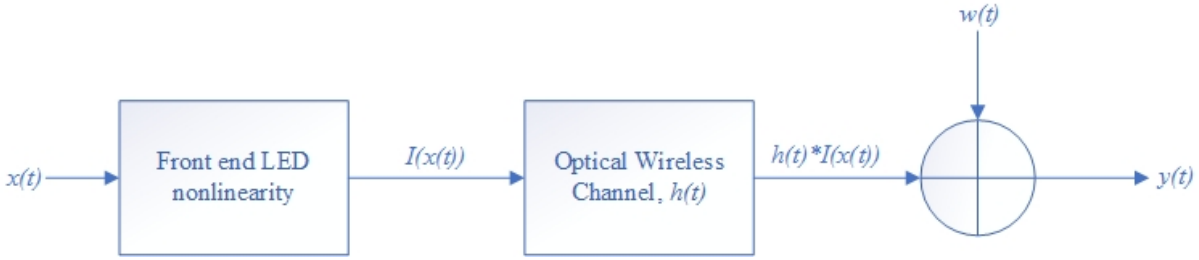

Figure 2.3. Optical wireless channel model is given.

where $h(t)$ *and* $w(t)$ stand for channel impulse response and additive noise in time domain, respectively. The symbol * indicates convolution operator and *I(t)* is the transmitted optical power. In VLC, noise terms can be classified into two categories: shot noise and thermal noise. Ambient light from other illumination sources, which does not carry data knowledge, produces shot noise. Additionally, thermal noise occurs in electronics. The sum of shot noise and thermal noise is supposed to be equivalent to $w(t)$. Ambient noise which is independent form $I(t)$ can be modeled as real valued zero mean Gaussian distribution $\mathcal{N}(0, \sigma^2)$. Thermal noise is not only independent of $I(t)$ but also independent of shot noise. Therefore, $w(t)$ is expressed as AWGN

$$\sigma^2 = \sigma_s^2 + \sigma_t^2 \tag{2.2}$$

where σ_s^2 and σ_t^2 are variances of the shot noise and thermal noise, respectively.

2.4 Modulation Techniques

Basic single-carrier pulse modulation schemes such as multi-level pulse amplitude modulation (M-PAM), multi-level pulse modulation (M-PPM) and pulse-width modulation (PWD) is usually adopted in optical communication system with IM/DD [7]. Large delay spread in the optical indoor wireless channel is the main problem of these modulation techniques under detrimental ISI which is limiting their output at high data rate as well as bit error rate performance. As an alternative way, multi-carrier modulation technique, orthogonal frequency division multiplexing (OFDM) becomes an attractive frame for high-data-rate visible light communication. This is due to the inherent robustness of OFDM to dispersion in the optical channel, which results in inter-symbol interference (ISI). This was also one key reason for the use of OFDM in RF communication [25]. Figure 2.4 depicts the frequency spectra of single carrier and multi carrier transmission.

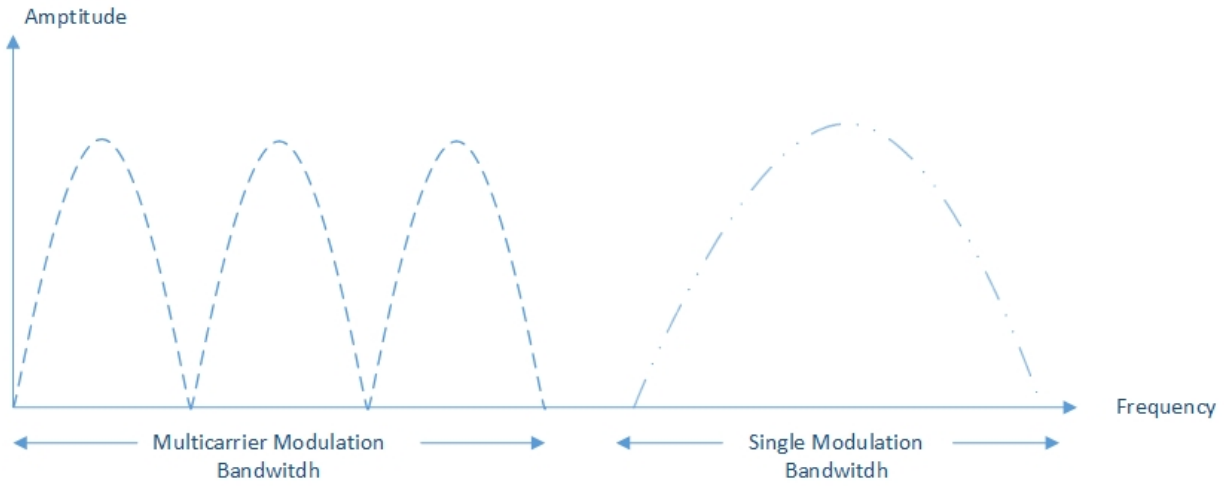

Figure 2.4. Illustration of frequency spectra formats of multi-carrier (on the left) and single carrier (on the right)

2.4.1 Multi- Carrier Modulation Technique: M-QAM O-OFDM

OFDM has been accepted as an effective method which can divide high data transmission into multiple lower speed data transmission via multiple sub-carrier channels. Distributed data across several orthogonal subcarrier channels results in high data rates via multiple parallel low-speed channels. Therefore, OFDM is able to effectively mitigate ISI [5,25]. As mentioned before, IM/DD is adopted in VLC. Amplitude of the optical OFDM signals must be non-negative and real-valued because of the LED constrains. Thus, conventional RF OFDM schemes cannot be used for VLC. OFDM based techniques suggested in literature can be classified under two classes; DC-biased optical ODFM (DCO-OFDM) and asymmetrically clipped optical OFDM (ACO-OFDM). Hermitian symmetry is imposed on active subcarriers in both systems to produce real-valued time domain signal. In ACO-OFDM, every even subcarrier is set to zero, and in order to generate a unipolar signal, time domain signal is clipped at zero. In DCO-OFDM even and odd subcarriers are utilized for data transmission. The block diagram of DCO-OFDM transmission is illustrated in

Figure 2.5. At the transmitter (T_x), the input data is mapped onto complex symbols by M-QAM modulation for each subcarrier to generate the data symbols, $X = [X_1, X_2 , \quad .... \quad , X_{\frac{N}{2}-1}]$.

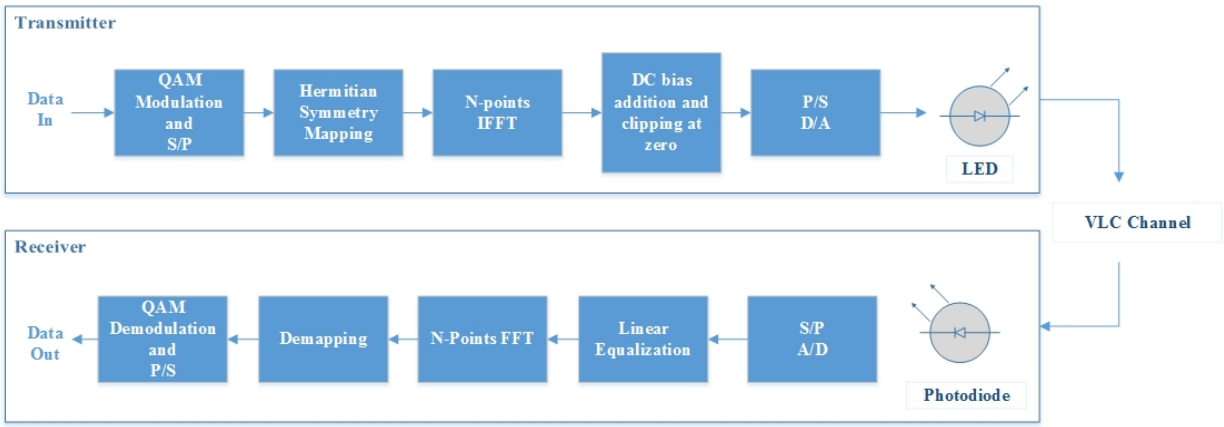

Figure 2.5. The structure of transmitter and receiver for O-OFDM

Hermitian symmetry is enforced on the active subcarriers of OFDM to ensure a real output signal. Total number of subcarriers is *N* and 0th and *N/2*th subcarriers are made zero to prevent the DC and complex-valued harmonic components [8,26]. Hermitian symmetry composition is shown in equation 2.2 and the symbol * denotes conjugate operation.

$$X_m = X_{N-m}^* \quad , \quad 1 \le m \le \frac{N}{2} - 1$$

$$x = \left\{0 , X_1, X_2, \ldots X_{\frac{N}{2}-1}, 0, X_{\frac{N}{2}-1}^* \ldots X_2^*, X_1^*\right\} \tag{2.2}$$

Later, inverse fast Fourier transform is applied to *x* in order to produce a time domain sequence which ends in N-point IFFT output of the OFDM symbol. IFFT process can be formulated as

$$x_k = \frac{1}{\sqrt{N}} \sum_{m=0}^{N-1} X_m \exp\left(\frac{j2\pi km}{N}\right) \tag{2.3}$$

where $k = 0,1 \ldots, N-1$. When N is large enough, $N \geq 64$, for instance, using the central limit theorem (CLT), x_m can be approximated as a Gaussian distribution with zero mean random variable, whose probability density function (pdf) is given by [6]

$$p_x(x) = \mathcal{N}(x; 0, \sigma^2) \triangleq \frac{1}{\sqrt{2\pi\sigma^2}} \exp\left(-\frac{x^2}{2\sigma^2}\right) \tag{2.4}$$

where σ^2 denotes the variance of x. Then, the time domain sequence is biased and clipped. The biasing and clipping range is decided using optical power condition and LED dynamic range, $[I_L I_H]$. The DCO-OFDM signal, $x_{DCO,k}$, is defined by

$$x_{DCO,k} = x_{clip,k} + I_{bias} \tag{2.5}$$

where clipped signal is defined by

$$x_{clip,k} = \begin{cases} -u_{lower} & x_k \leq -u_{lower} \\ x_n & -u_{lower} < x_k < u_{upper} \\ u_{upper} & x_k \geq u_{upper} \end{cases} \tag{2.6}$$

I_{bias} stands for biasing level which is added at the transmitter. Moreover, u_{lower} and u_{upper} are used for lower and upper bound of the clipping procedure and generally s related to the standard deviation of x_k [6]:

$$u_{lower} = a_1 \sqrt{E\{x_k^2\}}$$

$$u_{upper} = a_2 \sqrt{E\{x_k^2\}} \tag{2.7}$$

where E{.}shows the expected value. u_{lower} and u_{upper} bounds can be expressed in terms of dB as

$$u_{upper} = 10log_{10}({a_1}^2 + 1)\ dB$$

$$u_{lower} = 10log_{10}({a_2}^2 + 1)\ dB \tag{2.6}$$

In literature, to model clipping process, Bussgang theorem is used [27,6]. Equation (2.5) can be extended by Bussgang theorem to

$$x_{clip,k} = ax_n + d_n \tag{2.7}$$

where a is defined as an attenuation factor and d_n is the clipping noise. We can understand that the clipping operation in (2.6) attenuates the signal and leads to a clipping noise. Therefore, attenuation factor and clipping noise is defined in (2.7). x_n is uncorrelated with d_n. In addition, attenuation factor can be expressed as

$$a = \frac{E\{x_{clip,k}x_k\}}{E\{x_k^2\}} = \frac{1}{\sigma^2}\int_{-\infty}^{\infty} x_{clip,k}\, x_k\, p_x(x)\, dx \tag{2.8}$$

2.5 Summary

In this chapter, advantages and disadvantages of VLC system over RF communication systems were presented. The chapter has also given a summary of OWC transmission techniques for indoor applications. The fundamentals of OWC were discussed and building blocks for VLC systems were represented. Tradeoff between modulation techniques was discussed and the multi-carrier transmission technique OFDM was shown to be ideal for mitigating ISI for OWC applications. Moreover, in this chapter mathematical model for multi-carrier modulation scheme DCO-OFDM for VLC was presented represented. Clipping range was formulated as a function of variance of time domain signal x_n. The advantages of clipping were discussed.

CHAPTER 3

LOW DENSITY PARITY CHECK CODE

After rediscovery of LDPC codes in the mid 1990's LDPC has become an exciting research area for coding community. Lulby, Spielman, Richardson and Urbanke proved that there exist irregular LDPC codes which exceed the performance of the best Turbo codes. In recent studies, progressive edge growth (PEG) by Hu [15] construction technique can be seen in all LDPC code construction due to its outstanding performance. In this chapter, LDPC codes are introduced by the graphical model notation using Tanner Graph. Efficient encoder structure for upper triangulation construction is discussed. Also, optimality of the sum product algorithm and its mathematical formulization are also illustrated. In the ensuing two chapters puncturing and progressive edge growth construction are discussed.

3.1 Linear Block Codes

Linear block code uses an encoder that divides the information bits into message blocks of k information bits. Under certain rules, the encoder transforms each message block u into binary n-tuple codeword. Therefore, there are 2^k distinct codewords among 2^n possible n-tuple. A linear (n, k) block code is a subspace of n-tuples over $GF(2)$. Code rate is defined by $R = k/n$ and $R < 1$ because each codeword of length n carries k information bits [28]. In fact, binary summation of two codewords is also a codeword due to linearity. This property enables one to design generator matrix G, which reduces the encoding complexity. $The\ k$ linearly independent codewords can be design as the rows of $k\ x\ n$ generator matrix. The k linearly independent codewords as the row of $k\ x\ n$ generator matrix is given by

$$G = \begin{bmatrix} g_0 \\ \vdots \\ g_{k-1} \end{bmatrix} = \begin{bmatrix} g_{00} & \cdots & g_{0,n-1} \\ \vdots & \ddots & \vdots \\ g_{k-1,0} & \cdots & g_{k-1,n-1} \end{bmatrix} \tag{3.1}$$

where $\boldsymbol{g_i} = (g_{i0}, g_{i1}, \ldots, g_{i,n-1})$. Also, let $\boldsymbol{u} = (u_0, u_1, \ldots, u_k)$ be the message to be encoded. The codeword is defined by

$$\boldsymbol{v} = \boldsymbol{u} \,.\, G$$

$$= (u_0, u_2, \ldots, u_{k-1}). \begin{bmatrix} \boldsymbol{g_0} \\ \vdots \\ \\ \boldsymbol{g_k} \end{bmatrix} \tag{3.2}$$

$$= u_0\, \boldsymbol{g_0} + u_1\, \boldsymbol{g_1} + \ldots + u_{k-1}\, \boldsymbol{g_{k-1}}$$

As it is seen from the equation (3.1), rows of G produce the (n, k) linear code C. Another important property of a linear block code that should be mentioned is that systematic format of codeword is divided into two parts, as shown in Figure 3.1, which are message and redundant parts. Encoder attaches extra $(n - k)$ bits, which is the redundant part, to the transmitted data. The redundant part, which is also called parity bits, enables the code to combat with noisy channel. The other useful matrix H is called a parity check matrix of code C. Any vector in the row space of G is orthogonal to the $n - k = m$ rows of $(n - k)\ x\ n$ matrix H. That is, $v \in C$ if and only if $v.H^T = 0$ which also implies $G.H^T = 0$. Systematic expression of generator matrix and parity check matrix are $G = [\,P\ \ I_k]$ and $H = [\ I_{n-k}\ \ P^T\ ]$.

$$H = [\ I_{n-k}\ P^T\ ] = \begin{bmatrix} 1 & 0 & 0 & \cdots & 0 & p_{00} & p_{10} & p_{k-1,0} \\ 0 & 1 & 0 & \cdots & 0 & p_{01} & p_{11} & p_{k-1,1} \\ 0 & 0 & 1 & \cdots & 0 & p_{02} & p_{12} & p_{k-1,2} \\ & \vdots & & & & & & \vdots \\ 0 & 0 & 0 & \cdots & 1 & p_{0,n-k-1} & p_{1,n-n-1} & p_{k-1,k-1} \end{bmatrix} \quad (3.3)$$

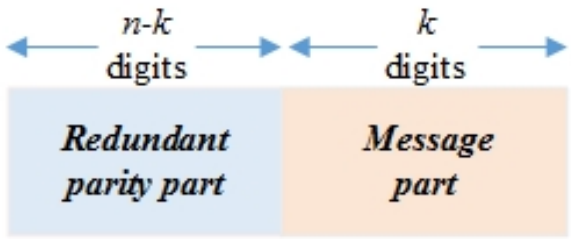

Figure 3.1. Systematic format of a codeword

3.2 Matrix and Graphical Representation of LDPC Code

LDPC codes fall under the category of linear block codes. Hence, it uses parity check equation $cH^T = 0$. The difference is that parity check matrix is a sparse matrix in which has a small density of 1 entries as compared with 0 entries. Initially, LDPC codes are constructed by a sparse parity check matrix and then a generator matrix is formed. *H* can be expressed as an $m \times n$ sparse matrix where m and n are used for the number of parity check equations and block length, respectively. The number of 1's in each row defines row weight, w_r, and the number of 1s in each column defines the column weight $w_c = w_r(n/m)$ where $w_c \ll m$. Code rate is in terms of weights $R = 1 - w_c/w_r$, assuming that H is a full rank matrix [28]. As originally proposed by Tanner [12], LDPC codes is graphically represented by a bipartite graph also called Tanner graph. Tanner graph involves two vertices denoted with variable nodes and check nodes depicted in Figure 3.2. Each

connection between check node and the variable node corresponds to the element h_{ji} in H that is a 1. Further, the m rows of parity check matrix represent m check node connections and the n columns of parity check matrix represent n variable node connections. Total number of edges on Tanner graph is equivalent to the total number of 1s in the parity check matrix. It is rather obvious that the parity check matrices for LDPC codes are significantly larger than that shown in the example in Figure 3.2. However, the same structure is valid for larger LDPC codes. A cycle is a path through edges with same starting and ending points. The girth g is the smallest cycle on Tanner graph. In figure 3.2, $v_1 \rightarrow c_1 \rightarrow v_4 \rightarrow c_2 \rightarrow v_1$ is the path which makes smallest cycle. This is girth 4 Tanner graph. *v* and *c* represent variable and check node, respectively.

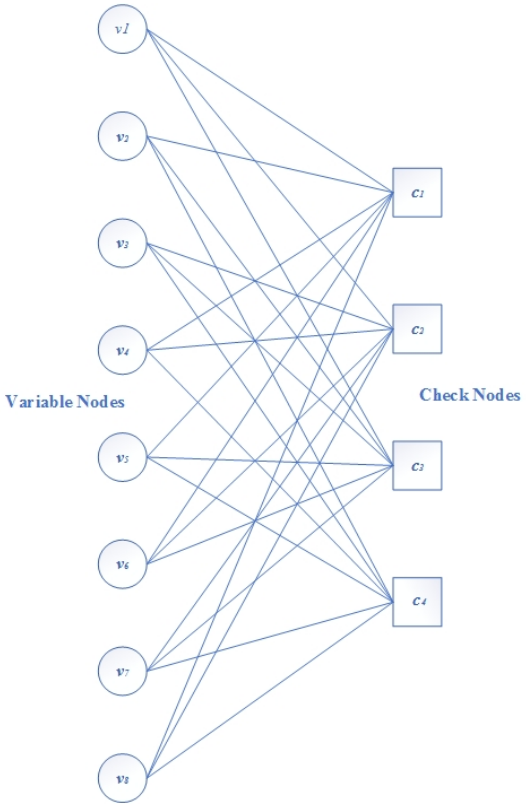

$$H = \begin{pmatrix} 1 & 1 & 0 & 1 & 1 & 1 & 0 & 1 \\ 1 & 0 & 1 & 1 & 0 & 1 & 1 & 1 \\ 1 & 1 & 1 & 0 & 1 & 1 & 1 & 0 \\ 0 & 1 & 1 & 1 & 1 & 0 & 1 & 1 \end{pmatrix}$$

Figure 3.2. Regular (3,6) LDPC code showing Tanner graph and H, parity check matrix

There are two types of LDPC codes in terms of density property; irregular and regular LDPC codes. For regular codes, row and column weights are constant, whereas irregular codes do not possess this feature. Weight notation is adopted for regular LDPC code as it is an easy notation to follow due to the constant weight feature of regular codes. In the literature, irregular codes are classified with degree distribution polynomials for the sake of consistency [29]. Generally, LDPC codes are characterized by a distribution pair $(\lambda(\mathrm{x}), \rho(x))$ [30]. $\lambda(\mathrm{x})$ and $\rho(x)$ are degree distribution polynomials (coefficients of the polynomials are non-negative real numbers). Also, the sum of the coefficients is 1 ($\lambda(1) = 1$) [29]. $\lambda(\mathrm{x})$ and $\rho(x)$ are given by

$$\lambda(\mathrm{x}) = \sum_{i=2}^{d_v} \lambda_i \, x^{i-1}$$

and

$$\rho(\mathrm{x}) = \sum_{i=2}^{d_c} \rho_i \, x^{i-1}, \tag{3.4}$$

respectively. d_v denotes the degree of the polynomial and λ_i depicts the portion of edges that are linked to degree *i* variable node. Similarly, d_c and $\rho(\mathrm{x})$ can be described for check nodes. If we have *n* variable nodes, the number of variable nodes with degree *i* is computed by

$$n \frac{\lambda_i / i}{\sum_{j \geq 2} \lambda_j / j} = n \, \frac{\lambda_i / i}{\int_0^1 \lambda(x) dx}. \tag{3.5}$$

Excepting that all parity check equations to be linearly independent, the relationship between degree distribution and code rate using (3.5) is given by

$$r(\lambda, \rho) = \frac{n-m}{n} = 1 - \frac{\int_0^1 \rho(x) \, dx}{\int_0^1 \lambda(x) \, dx} \tag{3.6}$$

Richardson *et al.* [13] proposed an effective degree distribution $\lambda(\mathrm{x}) = 0.1575x + 0.3429x^2 + 0.0363x^5 + 0.0590x^6 + 0.2790x^8 + 0.1253x^9$. The variable node degree distribution is derived in [13] for irregular parity check matrix. From (3.3), we can infer that the maximum and minimum

variable degrees are 10 and 2, and the non-zero entries for each degree can be calculated by its coefficient considering the length of code.

3.3 Encoding

There are many encoder structures that can be used for LDPC codes. In this research, greedy upper triangulation-based encoder will be the main approach. A direct method to realize the generator matrix in GF(2) is to apply Gaussian elimination and column permutations. This approach requires n^2 operation which increases the complexity dramatically. LDPC code can show outstanding error correction performance under large block lengths, n, condition. Under these circumstances, encoder gets prohibitively complex. Several researches have addressed this issue to create a more manageable encoder for LDPC. Richardson and Urbanke suggested an efficient encoding algorithm for LDPC codes in [32].

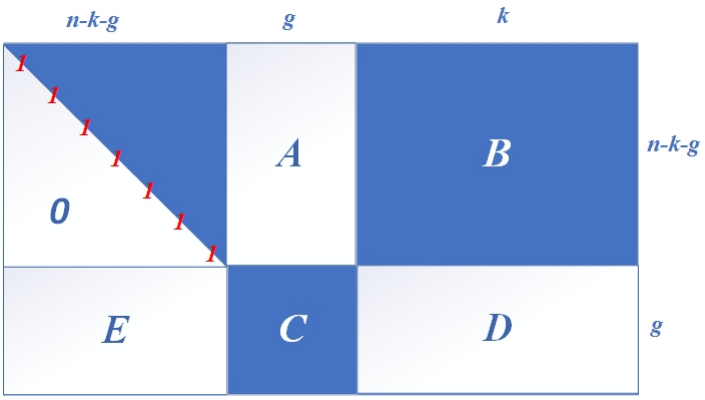

Figure 3.3. Approximate upper triangular form for H

According to [32], instead of finding generator matrix, H can be directly used to transform it into the desired upper triangular form depicted in Figure 3.3. The idea under the proposed encoding procedure is to keep the parity check matrix as sparse as possible by row and column permutations. Encoding can be separated under two main steps which are preprocessing and encoding steps. This

decomposition corresponds to a systematic form which is $H = (H_p \ H_s)$. Parity part of the new construction is $H_p = \begin{pmatrix} T & A \\ E & C \end{pmatrix}$ where T is a square and upper triangular matrix. As long as the operating elementary row events is in GF (2), swapping two rows or adding one row to another by modulo-2 operation will result in the same codeword set as the original matrix. Further, it remains sparse. Finally, H is conformed such that the matrix *T* is an *(n-k-g) x (n-k-g)* matrix*, A* is an *(n-k-g) x g* matrix, *B* is an *(n-k-g) x k* matrix*, E* is an *g x (n-k-g)* matrix*, C* is size of *(g x g)* matrix*,* and finally *D* is an (*g x k)* matrix*.* Basically, *H* is partitioned into six sub-matrices. To solve the system equation, we can eliminate the matrix *E* by premultiplying by $\begin{pmatrix} I & 0 \\ -ET^{-1} & I \end{pmatrix}$, which will yield

$$\begin{pmatrix} T & A & B \\ 0 & C - ET^{-1}A & D - ET^{-1}B \end{pmatrix} \tag{3.7}$$

System equation $Hv^T = 0^T$ can be directly solved by (3.7) for parities in $v = (p_1, p_2, s)$. Here, we have two important equations

$$Tp_1^T + Ap_2^T + Bs^T = 0^T$$

$$(C - ET^{-1})p_2^T + (D - ET^{-1}B)s^T = 0^T \tag{3.8}$$

$\emptyset = C - ET^{-1}A$ is an invertible sub-matrix, implying that H_p is also invertible. Note that any particular matrix is invertible and non-singular if and only if its determinant is non-zero. Here calculations are considered for the determinant in GF (2) so that the algebraic calculations will not lead any non-binary result. Next step will be deciding p_1 and p_2 from a given *s*. After some computations, it can be shown that

$$p_2^T = -\emptyset^{-1}(D - ET^{-1}B)s^T$$

$$p_1^T = -T^{-1}(Ap_2^T + Bs^T) \tag{3.9}$$

As a result, the required codeword with a given message s is created with parities p_1^T and p_2^T. When the operation is observed we can clearly see that complexity is reduced with the proposed method [32]. Overall the complexity for p_1 is of the order $O(n + g^2)$while for p_2 the complexity is of the order $O(n)$. The gap, g has an important role in the complexity analysis. Greedy upper triangulation aims to find the smallest possible g during encoding. Flow chart of greedy algorithm is provided in Figure 3.4.

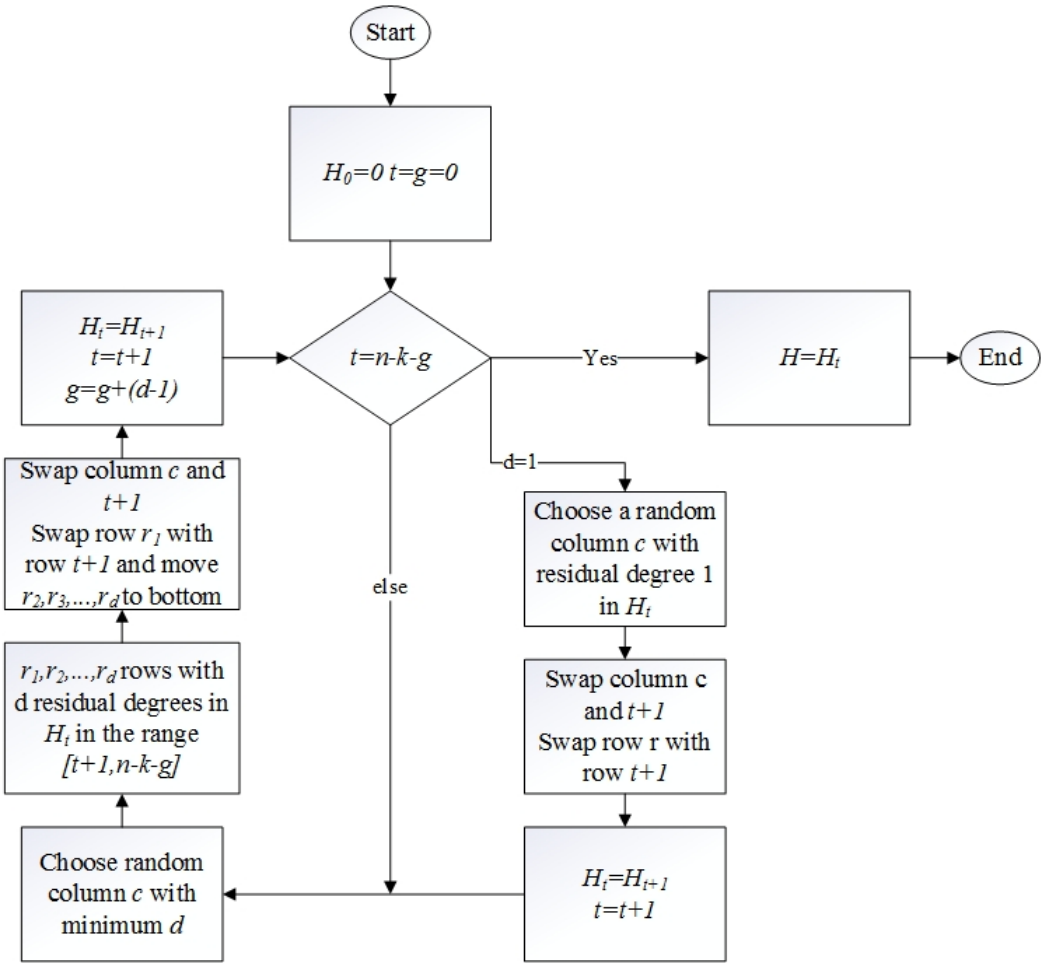

Figure 3.4. Greedy algorithm flow chart

3.4 Iterative Decoding of LDPC Codes

As mentioned in Chapter 1, Gallager proposed an iterative decoding algorithm for LDPC codes. LDPC decoding entails an iterative decoding algorithm called *message-passing*. In message passing algorithm, messages are exchanged through edges and calculated at nodes. The basic iterative method is known alternatively as belief propagation, message passing algorithm, and bit flipping algorithm. These algorithms underscore the type of information that is passed or the type of operation that is executed at the nodes. In message passing, each variable node passes the knowledge of its variable to the check nodes. After that, check nodes store the information and return back to the variable nodes. Subsequently, variable nodes update their knowledge and then report back to check nodes until decoder decides the correct codeword has been decoded. If the total sum is passed to the next node, some values will be considered twice. Because of that, only new information, called extrinsic information, is passed to the neighboring nodes.

In this chapter our main concern is the sum-product algorithm (SPA). Sum-product algorithm (also known as belief propagation) is a probabilistic decoding algorithm using the input bit probabilities called the *a priori* probabilities for the received bits, which are known in advance. The goal of the sum-product decoding is to estimate the optimal value for each given bit. This is known as the maximum a-posteriori (MAP) decoding which maximizes a posteriori probability. In the decoder, a priori probabilities return a posteriori probabilities (APP). Assuming equal probabilities for binary transmission, APP can be calculated by

$$Pr\,(\,v_i = 1 \mid y) \tag{3.10}$$

where v_i is the *i*th coded bit and y is the received word. APP also can be expressed by log likelihood ratio (LLR)

$$L(v_i) = log\left(\frac{p(v_i=0 \mid y)}{p(v_i=1 \mid y)}\right) \tag{3.11}$$

During the iterative process of sum-product algorithm, extrinsic information is obtained after first iteration. Figure 3.5 shows details of how extrinsic information is evolved. In the first half iteration, all information from v_1 is passed to c_2 except the information c_2 already carries. After first iteration is completed, second half iteration happens for the opposite direction on the graph under the same rules.

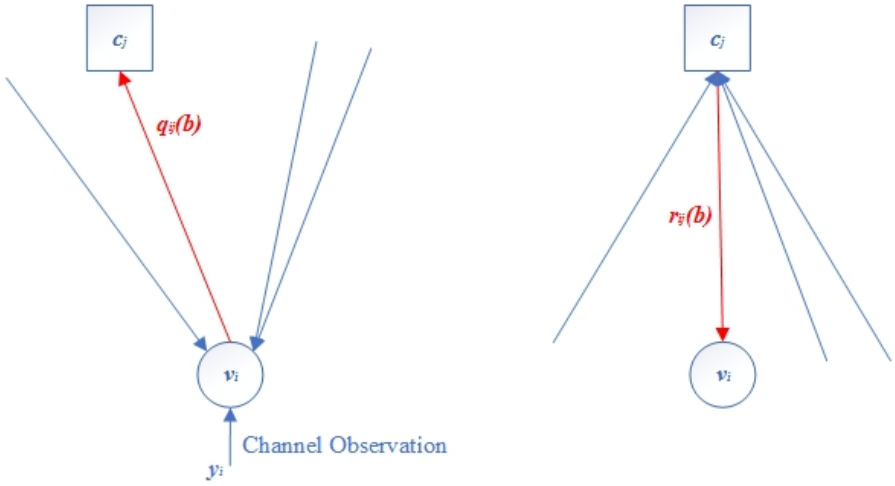

Figure 3.5. First half iteration and second half iteration in Message-Passing Algorithm

For simplicity, following notation is introduced

- ✓ V_j = variable nodes connected to jth check node
- ✓ $V_{j\backslash i}$ = $\mathrm{V_j} - i$th variable node (ith variable is not taken into calculation)
- ✓ C_j = check nodes connected to jth variable node
- ✓ $C_{i\backslash j} = C_j - j$th check node ($j$th check is not taken into calculation)
- ✓ $q_{ij(b)}$ = message from V_i to C_j regarding $P(v_i = b)$
- ✓ $r_{ji(b)}$ = message from C_j to V_i

- ✓ i, j stands for $h_{ij} = 1$

Probability domain sum-product algorithm was introduced by Gallager; however, the algorithm has many multiplications causing computational complexity and numerical instability. Hence a log domain form of SPA is considered. The required LLRs are

$$L(q_{ij}) = \log\left(\frac{q_{ij}(0)}{q_{ij}(1)}\right)$$

$$L(r_{ji}) = \log\left(\frac{r_{ji}(0)}{r_{ji}(1)}\right)$$

$$L(Q_i) = \log\left(\frac{Q_i(0)}{Q_i(1)}\right) \tag{3.12}$$

Using tanh rule, which is

$$tanh\left[\frac{1}{2}\log\left(\frac{p_0}{p_1}\right)\right] = p_0 - p_1 = 2p_1, \tag{3.13}$$

LLRs from (3.12) can be extended by

$$tanh\left(\frac{1}{2}L(r_{ji})\right) = \prod_{i' \in V_{j\backslash i}} \tanh\left(\frac{1}{2}L(q_{i'j})\right) \tag{3.14}$$

where $L(q_{ij}) = 2y_i/\sigma^2$ can be assign as an initialization step for AWGN channel. To reduce the complexity of (3.14), let

$$L(q_{ij}) = \alpha_{ij}\beta_{ij}$$

$$\alpha_{ij} = sign\left[L(q_{ij})\right]$$

$$\beta_{ij} = \left|L(q_{ij})\right| \tag{3.15}$$

So (3.12) may be rearranged as

$$tanh\left(\frac{1}{2}L(r_{ji})\right) = \prod_{i' \epsilon V_{j\backslash i}} \alpha_{i'j} \prod_{i' \epsilon V_{j\backslash i}} tanh\left(\frac{1}{2}\beta_{i'j}\right) \tag{3.16}$$

Then, we have

$$L(r_{ji}) = \prod_{i'} \alpha_{i'j} \; . 2tanh^{-1} \prod_{i'} \tanh\left(\frac{1}{2}\beta_{i'j}\right)$$

$$= \prod_{i'} \alpha_{i'j} \; . 2tanh^{-1} \; log^{-1} \; log\left(\prod_{i'} tanh\left(\frac{1}{2}\beta_{i'j}\right)\right)$$

$$= \prod_{i'} \alpha_{i'j} \; . 2tanh^{-1} log^{-1} \sum_{i'} log\left(tanh\left(\frac{1}{2}\beta_{i'j}\right)\right)$$

$$= \prod_{i' \epsilon V_{i\backslash j}} \alpha_{i'j} \; \phi^{-1}\left(\sum_{i' \epsilon V_{i\backslash j}} \phi(\beta_{i'j})\right) \tag{3.17}$$

where $\phi(x)$ is defined

$$\phi(x) = -\log\left(\tanh\left(\frac{x}{2}\right)\right) = \log\left(\frac{e^x + 1}{e^x - 1}\right).$$

Using the fact that $\phi\big(\phi(x)\big) = x$, $\phi^{-1}(x) = \phi(x)$ as long as $x > 0$. Using a lookup table makes the calculation of $\phi(x)$ easier. In [1], Gallager proposed updating equations for the probability domain sum-product algorithm, which are $q_{ij}(0) = K_{ij}(1 - P_i) \prod_{i' \epsilon V_{i\backslash j}} r_{j'i}(0)$ and $q_{ij}(1) = K_{ij} \, P_i \prod_{j \epsilon V_{i\backslash j}} r_{j'i}(1)$. If (3.17) is divided by these equations updating equations for nodes will be

$$L\big(q_{ij}\big) = L(v_i) + \sum_{j' \epsilon V_{i\backslash j}} L(r_{i'j})$$

$$L(Q_i) = L(v_i) + \sum_{j' \epsilon V_{i\backslash j}} L\big(r_{ji}\big) \, . \tag{3.18}$$

Decoding continues until a fixed number of iteration is completed or halting requirement, $\hat{v}H = 0$, is satisfied.

Final step is about making hard decision on the estimated decode block, $\hat{v}_i$. The output value of the *i*th bit is 1 if

$$\hat{v}_i = \begin{cases} 1\ , & if\ L(Q_i) < 0 \\ 0\ , & otherwise \end{cases} \tag{3.19}$$

3.5 LDPC Code Construction

Most of the existing LDPC codes are constructed randomly by eliminating cycles of length 4 [33,34,35,36]. In the Tanner graphs of randomly constructed codes, sparsity has a major role to avoid short cycles. Therefore, random constructed LDPC codes have been used largely due to their great performance. However, it is not guaranteed that these codes will have a satisfactory shortest cycle. Note that the optimum girth size gives good minimum distance in the Tanner graphs, which makes iterative decoding possible in high SNR levels. In the simplest terms, the probability of picking an undesirable random graph is very high, and this issue is crucial while creating irregular Tanner graphs.

Progressive Edge Growth (PEG) construction algorithm is studied due to having a large girth in Tanner graph by structuring the connections between symbol and check nodes progressively. New edges are placed on the Tanner graph with minimum impact. When the optimum edge has been established, new edge will be updated on the graph, and the steps will continue with the next edges. PEG Tanner graph construction in LDPC codes has considerably better simulation results compare to the randomly constructed LDPC codes.

In the PEG algorithm, the fundamental concept is the maximization of the local girth while adding new edges to the Tanner graph. The first j symbol nodes are constructed on the Tanner graph with

the edges $E_{v_0} \cup E_{v_1} \cup \ldots E_{v_{j-1}}$, and $g^t = \min\{g_{v_0}, g_{v_1}, \ldots, g_{v_{j-1}}\}$ is the temporary girth in the current step with the same edges. Selecting the edges with a variable node v_j is significant since g^t should not be affected by the new edges in order to have a large girth. Furthermore, the PEG algorithm choses check nodes, which is not reachable from s_j in order not to create additional cycle.

PEG algorithm:

for variable node $v, j = 0: n-1$

for edge $k, k = 0: d_{v_j} - 1$

if $k = 0$

$E_{v_j}^0 :=$edge(c_i, v_j), where c_i is the check node with the lowest degree in the Tanner graph and $E_{v_j}^0$ is the first edge

else

expand the graph from s_j to depth l with the same graph settings, satisfying cardinality $\bar{N}_{v_j}^l = \emptyset$ and $\bar{N}_{v_j}^{l+1} = \emptyset$, or else $\bar{N}_{v_j}^l$ halts growing, later $E_{v_j}^k :=$edge(c_i, v_j) , the k th edge with the lowest degree between nodes, chosen from cardinality $\bar{N}_{v_j}^l$

end

end

Where the $:=$ denotes assignment in the algorithm, and $N_{v_j}^l = V \backslash \bar{N}_{v_j}^l$ where $\bar{N}_{v_j}^l$ is the complement of $N_{v_j}^l$, and V is the vertices(nodes) set between $V = V_c \cup V_v$.

In brief, a method constructing large girth Tanner graphs with Progressive edge algorithm optimizes the location of the new edges with specific variable nodes. Also, PEG algorithm is used for constructing regular and irregular LDPC codes.

3.6 Puncturing of LDPC Codes

In error correcting codes, a fixed rate is generally chosen, and rate compatible codes lets the coding in different rates with a general encoder/decoder structure [16]. The most popular form of making this type of code is to use puncturing, which omits some of the parity bits to reach different code rates. Puncturing is a tradeoff between performance and code rate. For LDPC, this causes an additional problem. Higher-rate codes will have different iterative thresholds in the decoding part [37]. The method to accommodate puncturing is relatively simple. Let R be the code rate for the system, and let R' be the desired code rate after the puncturing process. Obviously, $R' > R$. In puncturing, the location of punctured symbols is known in the receiver. For puncturing purposes, the randomly chosen bits are punctured, and these bits are nullified in the decoder. Therefore, the knowledge of punctured symbols is not sent through the Tanner graph. Generally, random puncturing is employed with seeds. Additionally, prior research has offered some insight into the impact puncturing patterns. OFDM modulation requires more freedom in puncturing. In general, random puncturing is preferred in OFDM. Figure 3.7 describes performance difference between LDPC and punctured LDPC codes.

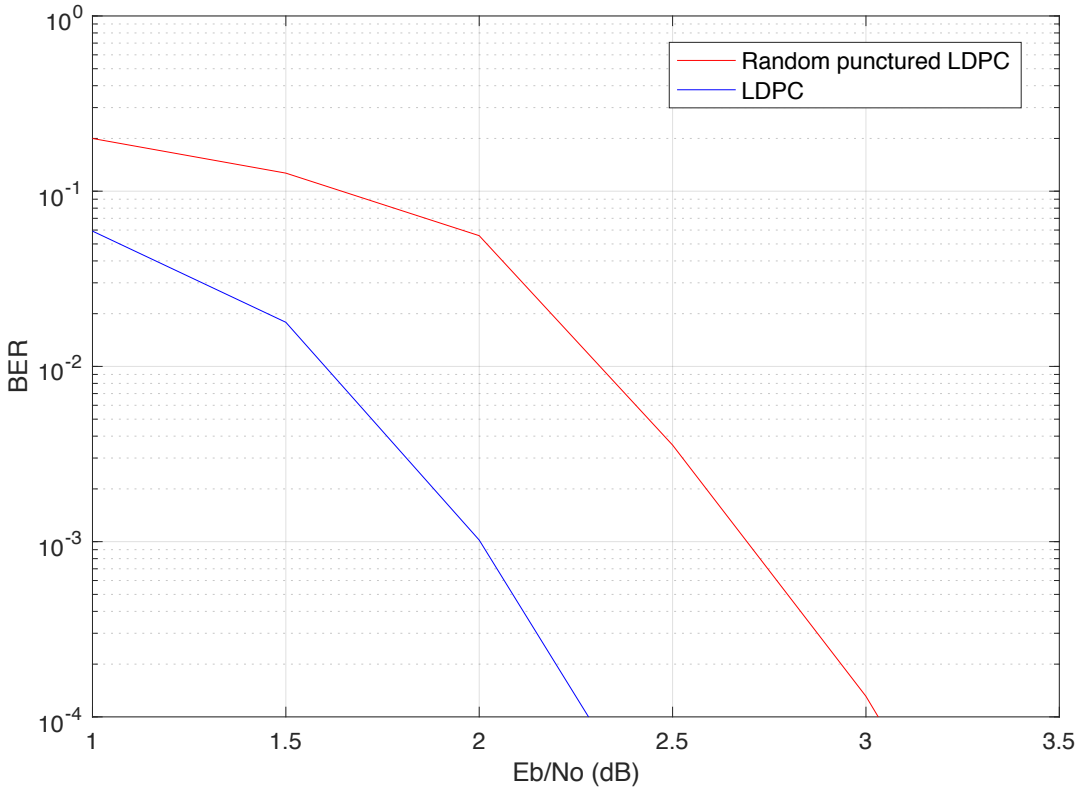

Figure 3.6. BER performance of LDPC codes with block length of 1008. Red curve depicts 0.6 rate punctured LDPC code. Blue curve is the original half rate LDPC code.

3.7 Conclusion

In this chapter, progressive constructed Tanner graphs and rate-compatible low-density parity check codes (LDPC) were investigated. Efficient encoding was satisfied by applying greedy upper triangulation-based encoder and iterative decoding algorithm. For decoding purposes, sum product algorithm (belief propagation) was chosen. This algorithm is a probabilistic decoding algorithm that uses the *a priori* probabilities for the received bits to estimate the optimal decision regarding the information bit. In the construction part of the code, Progressive Edge Growth (PEG) construction algorithm was utilized since this algorithm has large girths in the Tanner graph due

to using progressive structuring. Lastly, rate compatible LDPC code was studied using random puncturing.

CHAPTER 4

SYSTEM MODEL AND SIMULATION RESULTS

The objective of this study is to assess the potential of LDPC in mitigating the detrimental impact of clipping noise in DCO-OFDM systems. Reed-Solomon (RS) and LDPC coding-based schemes are incorporating with block expansion and puncturing in order to compensate non-linear distortion caused by the double-sided clipping method in LED-based OFDM system. Both coding schemes allow the system to reduce the magnitude of the transmitted signal and to regulate clipping process at the transmitter via the use of puncturing. Moreover, LDPC which is well-known error correction code can cope with the detrimental impacts of noise and channel distortion. Besides, RS coding scheme which can reach the maximum possible distance is compared with LDPC coding scheme. The performance of the LDPC and RS encoded DCO-OFDM systems in the presence of the double-sided clipping is assessed in terms of BER which is also defined as a function of the electrical bit energy to noise power ratio Eb/No. The impact of the signal bias on the useful signal energy is denoted by $d_{bias} = \frac{\sigma^2_{x_{clip,k}} + I^2_{bias}}{\sigma^2_{x_{clip,k}}}$ where I_{bias} is added at transmitter as a biasing level, and $x_{clip,k}$ is the signal after clipping. While the clipping range and signal biasing is studied, the parameters suggested in [38] are used to compare the BER performance of the two coding systems. The BER performance of the double-sided clipped LDPC and RS coded systems are verified through Monte-Carlo simulation for various normalized clipping levels. Also, all simulations corresponding to the LDPC codes are constructed with the progressive edge growth (PEG) algorithm.

Here, in order to recover the power efficiency and adapt to the linear characteristics of the LED, the biased time domain signals are clipped at $u_{lower} = a_{lower}\sigma_x$ and $u_{upper} = (5 - a_{lower})\sigma_x$. No clipping can be defined when upper and lower clipping levels are set to infinity. Also, the biasing level is set to $I_{bias} = a_{lower}\sigma_x$. We started by investigating scaling factor a_{lower} to analyze the impact of various clipping scenarios on LDPC and RS coded DCO-OFDM. The result is illustrated in Figure 4.1.

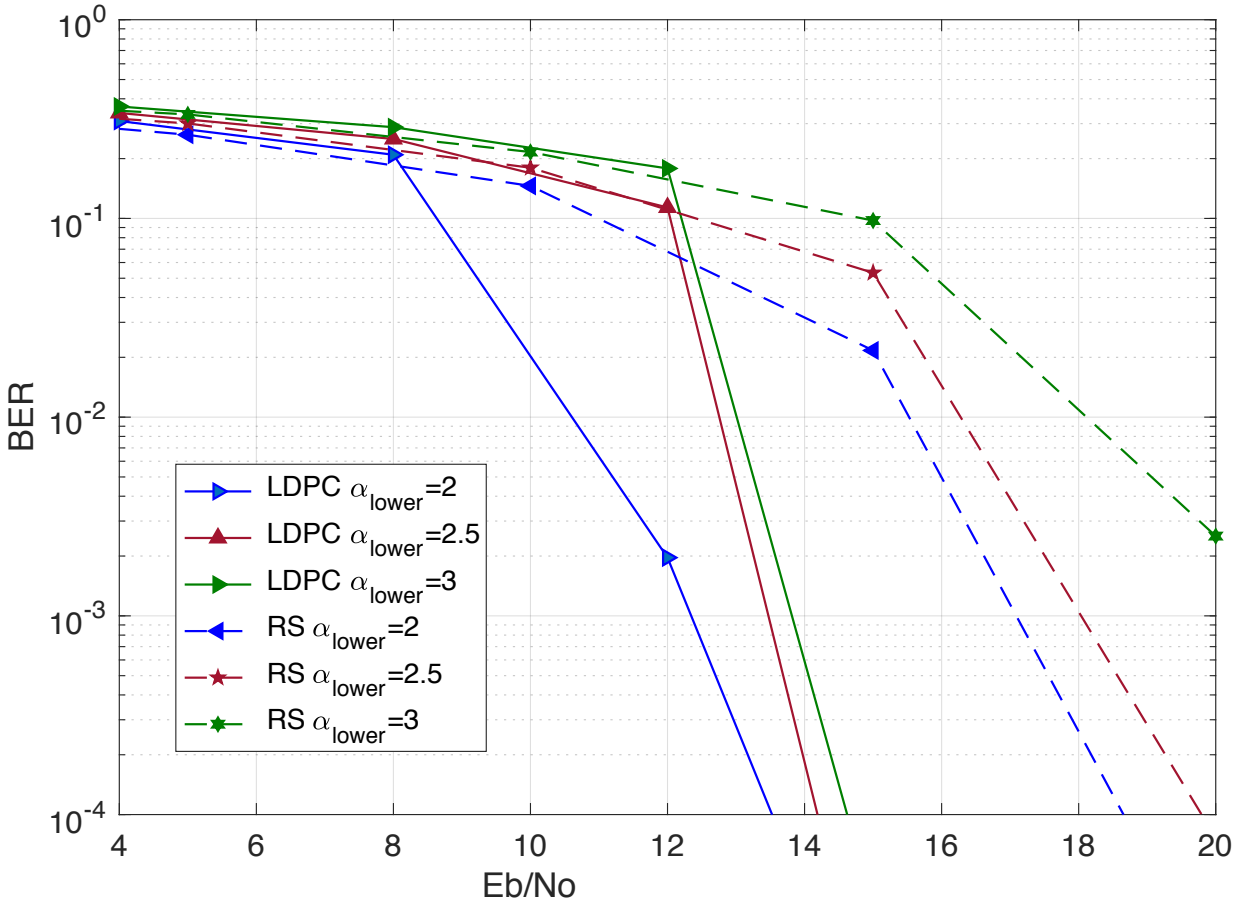

Figure 4.1 16-QAM bit error rate performance of LDPC coded DCO-OFDM vs RS encoded DCO-OFDM in AWGN channel for different clipping ranges.

For LDPC, the transmitted DCO-OFDM signal with IFFT/FFT size $N = 512$ is modulated by 16-QAM. A regular (3,6) LDPC code with length $N = 1020$ and rate $R = 1/2$ is used for the simulation where the maximum number of iteration of belief propagation algorithm is set to 100 in Figure 4.1. The data block with the length $K = 510$ is converted into codeword with the length $N = 1020$. After Hermitian symmetry is employed, first and $N/2$ th subcarriers are set to zero. Same IFFT/FFT length and modulation order are used for the RS (15,8) block code for fair comparison. In all simulations, solid lines correspond to the LDPC results while dashed lines correspond to the RS results.

Such cases are depicted in Figure 4.1, where the scaling factor a_{lower} is set at 2, 2.5, and 3. As a_{lower} is increased, implying higher biasing level, a degraded performance for both LDPC and RS coding schemes is observed. Moreover, 16 QAM LDPC coded system outperforms RS coded system even under severe clipping conditions. On the other hand, LDPC causes a considerable increase in complexity and energy consumption. As can be seen in Figure 4.1, the optimum clipping level is reached at $u_{lower} = 2\sigma_x$ for both coding systems, and it will be used in the next simulations.

The alternative way for avoiding the detrimental impact of clipping distortion was proposed recently. The approach uses puncturing to avoid large variations in the OFDM signal, which results in a smaller peak value. This technique enables both LDPC and RS codes to control clipping probability by decreasing the magnitude of the time domain signal due to puncturing of the redundancy of the codes. In Figure 4.2, $u_{lower} = 2\sigma_x$ is taken into consideration as an optimum clipping range from the first simulation result.

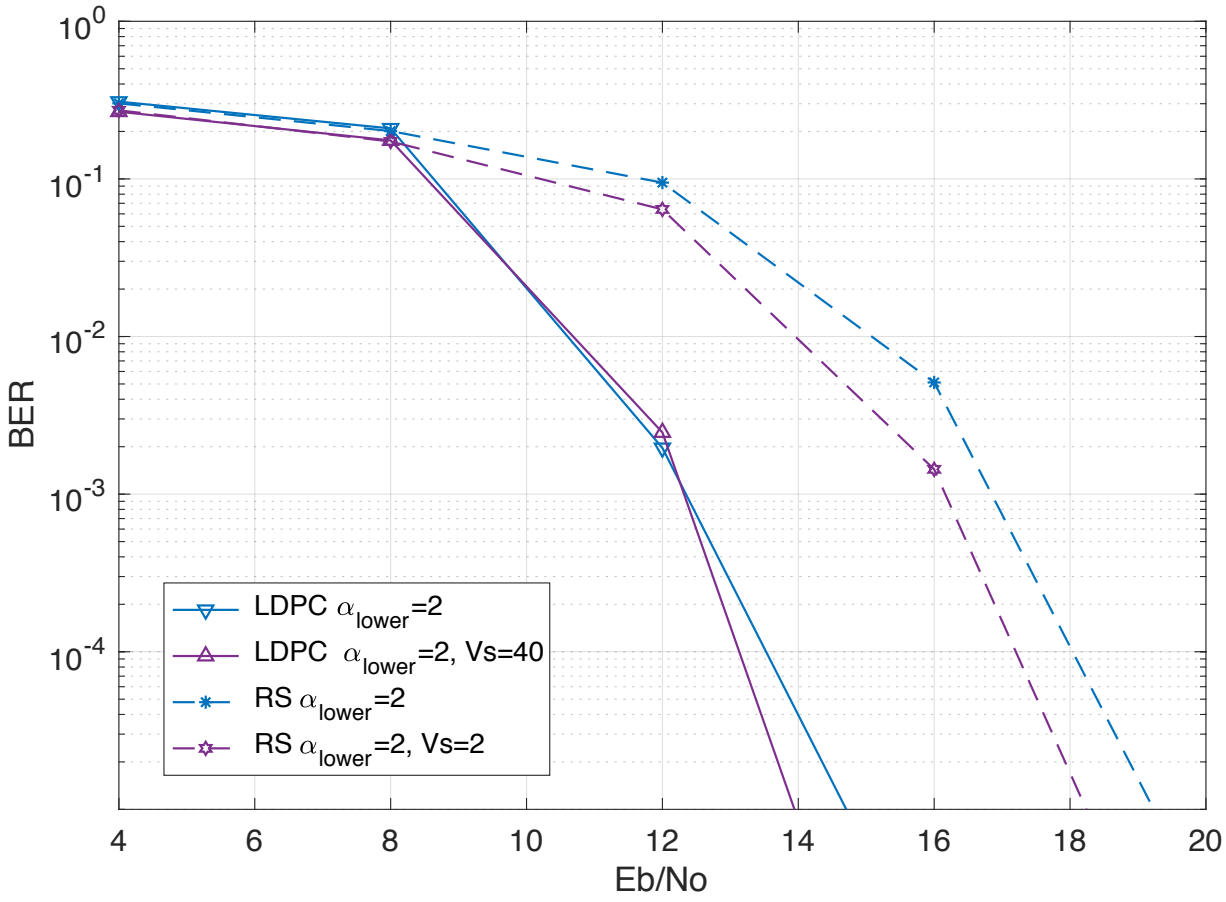

Figure 4.2. 16-QAM Bit error rate performance of LDPC coded DCO-OFDM vs RS encoded DCO-OFDM in AWGN channel with puncturing.

Puncturing is used to achieve different code rates by normalizing energy per bit with respect to the coding rate for $\frac{K}{N-V_s}$ where V_s denotes the number of punctured symbols. The output of the encoder is exposed to different number of puncturing. In RS structure, 17 consecutive codewords with the length of 15 are considered to have the same subcarrier size as in the LDPC structure.

Punctured symbols in data vector are set to zero in the corresponding OFDM subcarriers. More specifically, when $V_s = 20$, LDPC shows 0.4 dB gain at the target SNR of 10^{-4}. Its counterpart RS shows 0.75 dB gain at target SNR of 10^{-4} when $V_s = 2$. In the two techniques, the number

of punctured symbols is arranged to reach the same coding rate for fair comparison. In general, LDPC outperforms RS coding by a large margin for all SNR levels.

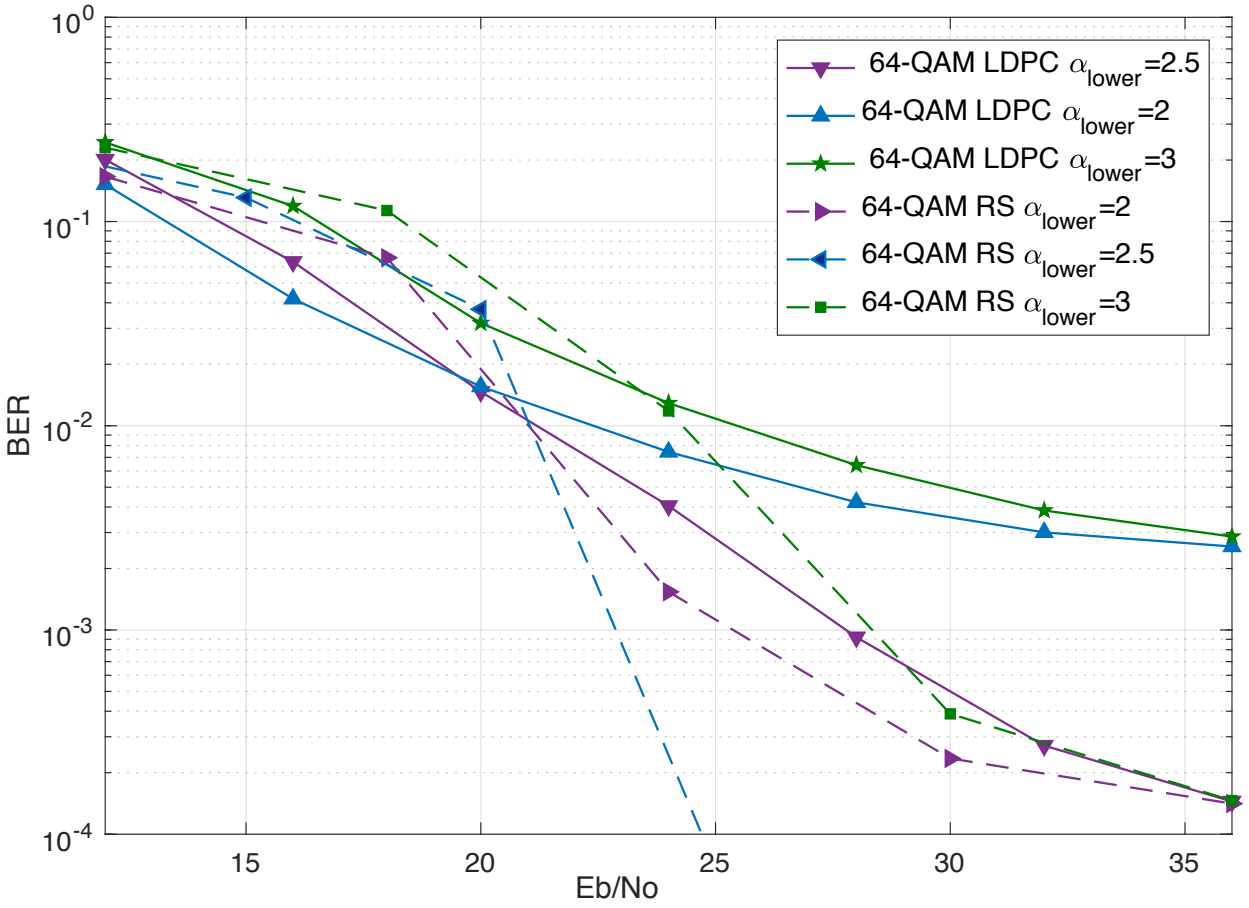

Figure 4.3. 64-QAM Bit error rate performance of LDPC coded DCO-OFDM vs RS encoded DCO-OFDM in AWGN channel for different clipping ranges.

In Figure 4.3, 64-QAM simulation results are provided with IFFT/FFT size N=512 and higher modulation order (64 QAM). Half rate LDPC block length is 1530. To ensure same subcarrier size as in LDPC structure, for (63,31) RS code, 4 consecutive codewords with the length of 63 are put in series to modulate the first 252 subcarriers. 4 residual subcarriers are set to zero. For the resulting plot (see Figure 4.3) optimum clipping range for LDPC and RS is attained when $u_{lower} = 2.5\sigma_x$. When compared with the 16-QAM results, it can be seen that optimum clipping range is changed.

This result proves higher order modulation is more vulnerable to clipping due to the shrinking of the decision region. Hence, for a given biasing setup at the transmitter front-end, the noise caused by the non-linear clipping distortion affects the BER performance of higher modulation, as presented in Figure 4.3, in a more profound manner. In addition, it has been found that LDPC suffers from the impact of clipping in higher modulation.

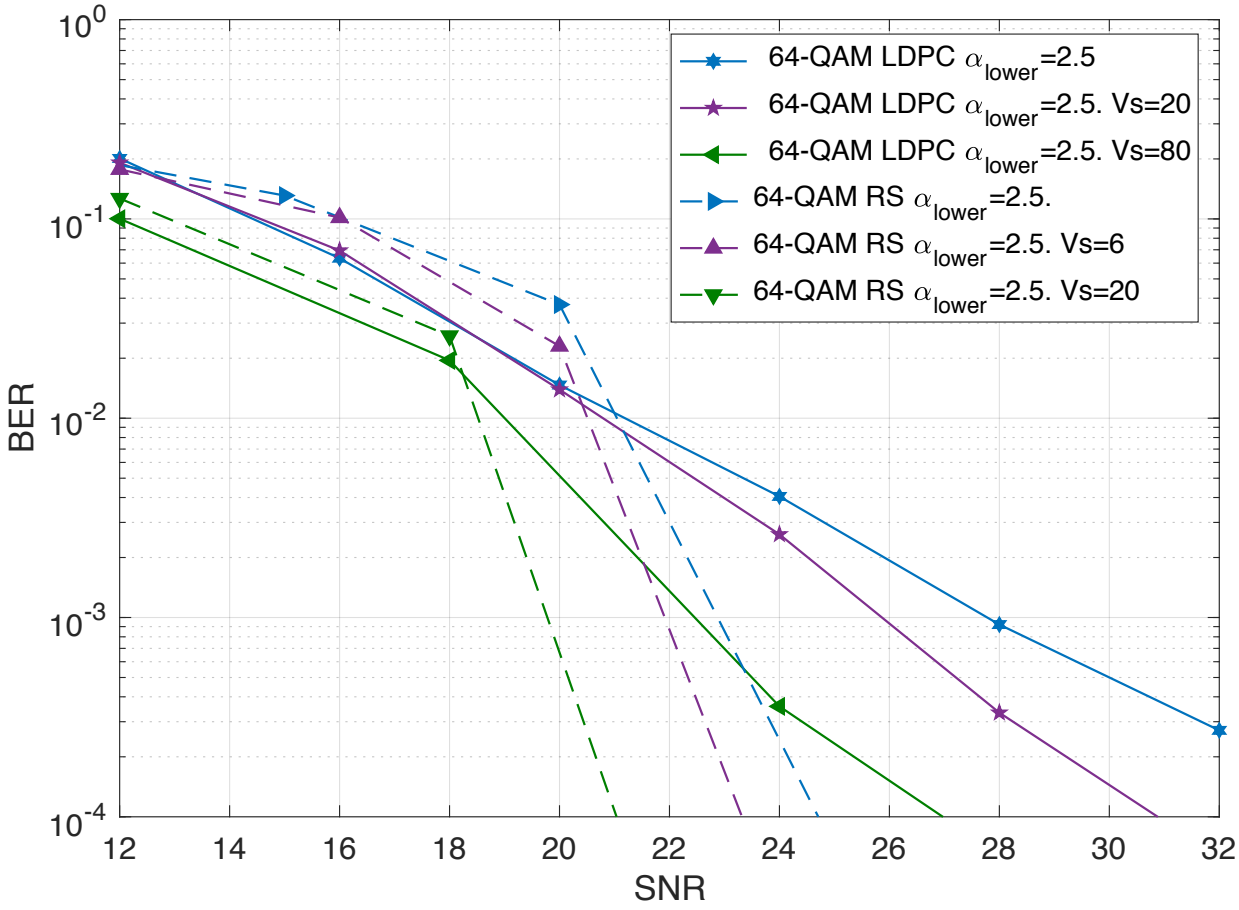

Figure 4.4. 64-QAM bit error rate performance of LDPC coded DCO-OFDM vs RS encoded DCO-OFDM in AWGN channel with different puncturing rates.

Lastly, puncturing approach is for 64-QAM is studied in Figure 4.4. $a_{lower} = 2.5$ is chosen as an optimum value. The plot shows that punctured BER performance of RS coded DCO-OFDM is

better than its un-punctured counterpart at the target BER of $BER = 10^{-4}$ by approximately 3.7 dB when $V_s = 20$ is used. LPDC also offers several dB of performance enhancements when 80 punctured symbols are considered as compared with the 20 punctured symbols or no puncturing scenarios.

Finally, we observed that the punctured LDPC OFDM systems in the presence of clipping outperform their RS coded systems for low order modulation. For higher modulation levels, RS-coded systems are shown to be superior to their LDPC counterpart.

From the outcome of our investigation, it is possible to conclude that using puncturing on the redundancy carrying subcarriers in an OFDM system and correcting the clipping distortion by an efficient encoding and decoding algorithm result in improved BER performance of the system. Therefore, the proposed technique efficiently mitigates the clipping noise in DCO- OFDM based VLC systems.

CHAPTER 5

CONCLUSION

This thesis presented a comprehensive analysis of the BER performance in additive white gaussian noise of multicarrier modulation such as multi-level quadrature amplitude modulation (M-QAM) with DC-biased OFDM (DCO-OFDM) employing low density parity check coding and Reed Solomon coding. The presented framework assumed puncturing of the redundancy aiming to mitigate the impact of clipping noise at the transmitter by decreasing the number of active subcarriers in OFDM. Therefore, the severe impact of the non-linear clipping process was mitigated by the proposed technique.

Furthermore, we evaluated the performance of PEG constructed LDPC coded and RS coded DCO-OFDM under several parameters, such as biasing level, clipping level, modulation order, efficiency of puncturing, and different decoders in order to meet the optical power constraints of the front-end transmitter. First, for 16-QAM, various biasing and clipping levels were successfully investigated. It was shown that increasing the bias resulted in high electrical power and less clipping noise. Therefore, the optimum clipping range was suggested for LDPC and RS coded designs. While LDPC outperforms RS, the optimum clipping range did not differ. During simulations, tradeoff between complexity and performance was noted. The belief propagation algorithm which was used for LDPC caused an increase in the computational complexity as compared with RS systems. Using suggested optimum clipping range on puncturing, it was proved that puncturing improved BER because this process reduced the magnitude of the time domain signal at the transmitter. Higher order modulations are typically more vulnerable to the additive while Gaussian noise; therefore, non-linear clipping distortion severely affects BER performance

of higher order modulation. It was demonstrated via simulation that 64-QAM modulation schemes require a different clipping range than that of 16-QAM system for both RS and LDPC systems. Once again, clipping distortion was mitigated by puncturing of the OFDM symbols. Finally, it was shown that for higher modulation levels, RS coded systems outperform their LPDC counterparts for OFDM systems with clipping and puncturing. For lower order modulation, LDPC was proven to be superior to its RS counterpart.

REFERENCES

[1] A. G. Bell, W. G. Adams, Tyndall, and W. H. Preece, “Discussion on the photophone and the conversion of radiant energy into sound,” J. Soc. Telegraph Eng., vol. 9, no. 34, pp. 375–383, 1880.

[2] F. R. Gfeller and U. Bapst, "Wireless in-house data communication via diffuse infrared radiation," in Proceedings of the IEEE, vol. 67, no. 11, pp. 1474-1486, Nov. 1979.

[3] Y. Tanaka, S. Haruyama and M. Nakagawa, "Wireless optical transmissions with white colored LED for wireless home links," 11th IEEE International Symposium on Personal Indoor and Mobile Radio Communications. PIMRC 2000. Proceedings (Cat. No.00TH8525), London, 2000, pp. 1325-1329 vol.2.

[4] T. Komine, S. Haruyama and M. Nakagawa, "Performance evaluation of narrowband OFDM on integrated system of power line communication and visible light wireless communication," 2006 1st International Symposium on Wireless Pervasive Computing, 2006, pp. 6 pp.

[5] J. Armstrong and A. J. Lowery, "Power efficient optical OFDM," in Electronics Letters, vol. 42, no. 6, pp. 370-372, 16 March 2006.

[6] S. Dimitrov, S. Sinanovic and H. Haas, "Clipping Noise in OFDM-Based Optical Wireless Communication Systems," in IEEE Transactions on Communications, vol. 60, no. 4, pp. 1072-1081, April 2012.

[7] S. Dimitrov, S. Sinanovic and H. Haas, "Signal Shaping and Modulation for Optical Wireless Communication," in Journal of Lightwave Technology, vol. 30, no. 9, pp. 1319-1328, May1, 2012.

[8] C. He and J. Armstrong, "Clipping Noise Mitigation in Optical OFDM Systems," in IEEE Communications Letters, vol. 21, no. 3, pp. 548-551, March 2017

[9] N. Taherkhani and K. Kiasaleh, "Reed Solomon Encoding for the Mitigation of Clipping Noise in OFDM-Based Visible Light Communications," 2018 International Conference on Computing, Networking and Communications (ICNC), Maui, HI, USA, 2018, pp. 285-289.

[10] C. E. Shannon, "A mathematical theory of communication," in The Bell System Technical Journal, vol. 27, no. 4, pp. 623-656, Oct. 1948.

[11] R. Gallager, "Low-density parity-check codes," in *IRE Transactions on Information Theory*, vol. 8, no. 1, pp. 21-28, January 1962.

[12] R. Tanner, "A recursive approach to low complexity codes," in *IEEE Transactions on Information Theory*, vol. 27, no. 5, pp. 533-547, Sep 1981.

[13] D. J. C. MacKay and R. M. Neal, "Near Shannon limit performance of low density parity check codes," in Electronics Letters, vol. 32, no. 18, pp. 1645-, 29 Aug 1996.

[14] Sae-Young Chung, G. D. Forney, T. J. Richardson and R. Urbanke, "On the design of low-density parity-check codes within 0.0045 dB of the Shannon limit," in IEEE Communications Letters, vol. 5, no. 2, pp. 58-60, Feb 2001.

[15] Xiao-Yu Hu, E. Eleftheriou and D. M. Arnold, "Progressive edge-growth Tanner graphs," *Global Telecommunications Conference, 2001. GLOBECOM '01. IEEE*, San Antonio, TX, 2001, pp. 995-1001 vol.2.

[16] J. Hagenauer, "Rate-compatible punctured convolutional codes (RCPC codes) and their applications," in *IEEE Transactions on Communications*, vol. 36, no. 4, pp. 389-400, Apr 1988.

[17] D. G. M. Mitchell, M. Lentmaier, A. E. Pusane and D. J. Costello, "Randomly Punctured LDPC Codes," in *IEEE Journal on Selected Areas in Communications*, vol. 34, no. 2, pp. 408-421, Feb. 2016.

[18] D. Karunatilaka, F. Zafar, V. Kalavally and R. Parthiban, "LED Based Indoor Visible Light Communications: State of the Art," in *IEEE Communications Surveys & Tutorials*, vol. 17, no. 3, pp. 1649-1678, thirdquarter 2015.

[19] I. Hosako et al., "At the Dawn of a New Era in Terahertz Technology," in Proceedings of the IEEE, vol. 95, no. 8, pp. 1611-1623, Aug. 2007.

[20] N. Chi, H. Haas, M. Kavehrad, T. D. C. Little and X. L. Huang, "Visible light communications: demand factors, benefits and opportunities [Guest Editorial]," in IEEE Wireless Communications, vol. 22, no. 2, pp. 5-7, April 2015.

[21] World Health Organization (WHO), "Electromagnetic fields and public health", 2006, http://www.who.int/peh-emf/publications/facts/fs304/en/.

[22] S. Dimitrov and H. Haas, Principles of LED Light Communications: Towards Networked Li-Fi. Cambridge, U.K.: Cambridge Univ. Press, Mar. 2015.

[23] J. M. Kahn and J. R. Barry, "Wireless infrared communications," in Proceedings of the IEEE, vol. 85, no. 2, pp. 265-298, Feb 1997.

[24] J.G. Proakis and M. Salehi, Digital Communications (5th Ed.), McGraw Hill, 2008.

[25] A. J. Lowery and J. Armstrong, "Comparison of power-efficient optical orthogonal frequency division multiplexing transmission methods," *ACOFT/AOS 2006 - Australian Conference on Optical Fibre Technology/Australian Optical Society*, Melbourne, VIC, 2006, pp. 1-3.

[26] C. He and J. Armstrong, "Clipping Noise Mitigation in Optical OFDM Systems," in *IEEE Communications Letters*, vol. 21, no. 3, pp. 548-551, March 2017.

[27] J.J. Bussgang,"Cross-correlation function of amplitude-distorted Gaussian signals", Res. Lab. Elec., Mas. Inst. Technol., Cambridge MA, Tech. Rep. 216, March 1952

[28] S. Lin and D.J. Costello, Jr., Error Control Coding (2nd Ed.), Prentice Hall, 2004.

[29] T. J. Richardson, M. A. Shokrollahi and R. L. Urbanke, "Design of capacity-approaching irregular low-density parity-check codes," in *IEEE Transactions on Information Theory*, vol. 47, no. 2, pp. 619-637, Feb 2001.

[30] J. Huang, W. Zhou and S. Zhou, "Structured Nonbinary Rate-Compatible Low-Density Parity-Check Codes," in *IEEE Communications Letters*, vol. 15, no. 9, pp. 998-1000, September 2011.

[31] J. Hagenauer, E. Offer and L. Papke, "Iterative decoding of binary block and convolutional codes," in *IEEE Transactions on Information Theory*, vol. 42, no. 2, pp. 429-445, Mar 1996.

[32] T. J. Richardson and R. L. Urbanke, "Efficient encoding of low-density parity-check codes," in *IEEE Transactions on Information Theory*, vol. 47, no. 2, pp. 638-656, Feb 2001.

[33] T. J. Richardson and R. L. Urbanke, "The capacity of low-density parity-check codes under message-passing decoding," in IEEE Transactions on Information Theory, vol. 47, no. 2, pp. 599-618, Feb 2001.

[34] T. Richardson, A. Shokrollahi and R. Urbanke, "Design of provably good low-density parity check codes," 2000 IEEE International Symposium on Information Theory (Cat. No.00CH37060), Sorrento, 2000.

[35] M. G. Luby, M. Mitzenmacher, M. A. Shokrollahi and D. A. Spielman, "Improved low-density parity-check codes using irregular graphs," in *IEEE Transactions on Information Theory*, vol. 47, no. 2, pp. 585-598, Feb 2001.

[36] D. J. C. MacKay, "Good error-correcting codes based on very sparse matrices," *Proceedings of IEEE International Symposium on Information Theory*, Ulm, 1997.

[37] Jeongseok Ha, Jaehong Kim and S. W. McLaughlin, "Rate-compatible puncturing of low-density parity-check codes," in *IEEE Transactions on Information Theory*, vol. 50, no. 11, pp. 2824-2836, Nov. 2004.

[38] J. Armstrong and B. J. C. Schmidt, "Comparison of Asymmetrically Clipped Optical OFDM and DC-Biased Optical OFDM in AWGN," in *IEEE Communications Letters*, vol. 12, no. 5, pp. 343-345, May 2008.

BIOGRAPHICAL SKETCH

Merve Apalak is currently pursuing her Master of Science degree in Electrical Engineering at the Optical Communication Laboratory in the Eric Jonsson School of Engineering and Computer Science at The University of Texas at Dallas, Richardson, TX. She expects to graduate by August 2018 with 3.541. She received the Bachelor of Engineering degree in Electrical and Electronical from Erciyes University, Kayseri, Turkey, in 2014. During her Master's Degree she is fully granted by the Turkish Ministry of National Education. She will be attending PhD degree at the Optical Communication Laboratory in the Eric Jonsson School of Engineering and Computer Science at The University of Texas at Dallas, Richardson, TX in Fall 2018. Her current research interests include Visible Light Communication, Channel Coding, Error Correcting Codes, Optical Wireless Channel, Low Density Parity Check Codes, and Visible Light Communication Indoor Enhancement.

CURRICULUM VITAE

Merve Apalak
mxa167630@utdallas.edu
Dallas, TX 75248

EDUCATION

The University of Texas at Dallas August 2018 -
PhD: Electrical Engineering
The University of Texas at Dallas August 2016 – Summer 2018
MSc: Electrical Engineering GPA 3.54
Academic English Program, The University of Texas at Austin January 2016 – July 2016
Erciyes University, Kayseri, Turkey 2010 - 2014
BSc: Electrical Engineering GPA 2.68/4.0
Final Thesis: Obstacle Avoiding Robot

WORK EXPERIENCE

Intern – *Turkish Airlines Istanbul, Turkey* Summer, 2012
Intern – *Turkish Communications, Kayseri, Turkey* Summer, 2014

PROJECTS

Smart Pillow for Sleep Quality Spring 2017

- Designed a smart pillow with sensor sensing humidity, temperature and voice in order to see individual's sleeping quality

ECG Signal Classification Using Smartphone and Cloud Summer 2017

- Implemented Support Vector Machine on smartphone application to classify normal and abnormal heartbeat signal and used cloud for storage

AWARDS

Graduate Scholarship, Ministry of National Education, Turkey 2015
Teaching Assistant, The University of Texas at Dallas 2018

VOLUNTEER WORK AND ORGANIZATIONS

Head, Erciyes IEEE Student Community, Erciyes University 2010-2013

SKILLS

- Knowledge in C/C++ and Matlab